(Received 28 September 2023, Accepted 5 December 2023, Scheduled 13 December 2023)

Design of Wide Notched-Band Circular Monopole Ultra-Wideband Reconfigurable Antenna Using PIN Diodes Switches

Annu Tiwari[1], Dinesh Yadav[1,*], Purnima Sharma[2], and Manish Varun Yadav[3]

[1]*Department of Electronics & Communication Engineering*
Manipal University Jaipur, Jaipur, Rajasthan, India
[2]*Department of Electronics & Communication*
Institute of Engineering & Technology, GLA University, Mathura, India
[3]*Department of Aeronautical and Automobile Engineering*
Manipal Institute of Technology, Manipal Academy of Higher Education, Manipal, Karnataka, India

ABSTRACT: This communication presents the design of a circular monopole ultra-wideband (UWB) reconfigurable antenna with wide notched-band of 1 GHz which ranges from 5 to 6 GHz in UWB. The design involves a circular monopole antenna with embedded three thin slots (two vertical and one horizontal) and one rectangular slot at the top edge. The three p-i-n diodes are inserted in between vertical slots to control the flow of surface current in ON/OFF states. As a result, in all diodes' ON and OFF states, the designed antenna shows switching of its resonance in whole UWB to wide notched band UWB applications. The CST-microwave studio software is used to simulate the structure in time domain. The full modeling of reported reconfigurable antenna that includes reactive effects of the diode is achieved by ADS circuit simulator.

1. INTRODUCTION

Ultra-wideband (UWB) technology has emerged as a promising solution for high-speed wireless communication systems, catering to the ever-increasing demand for data-intensive applications [1]. UWB antennas are capable of transmitting and receiving data over a wide frequency range, enabling high-data-rate communication, precise localization, and radar imaging applications. However, the coexistence of various wireless communication systems operating in different frequency bands can result in interference, degrading the overall performance of UWB systems [2, 3]. To address this challenge, the integration of reconfigurable functionality into UWB antennas has gained considerable attention [4].

The monopole ultra-wideband reconfigurable antenna provides the capability to adjust and accommodate various operating scenarios. The antenna's resonance can be dynamically modified by employing PIN diode switches, enabling it to move between different frequency bands without the need for physical alterations to the antenna structure [5]. The antenna's flexibility to be reconfigured allows for the dynamic suppression of certain frequency bands, even those occupied by narrowband systems causing interference [6]. This reconfiguration ensures that the antenna maintains its wideband performance for UWB communication. The inclusion of this characteristic holds significant significance in guaranteeing dependable and uninterrupted connection within a wide range of wireless settings [7, 8].

The proliferation of UWB antennas can be attributed to the increasing need for high-speed wireless communication systems. UWB technology enables the rapid transmission of data across a broad spectrum of frequencies, facilitating its utilization in a diverse range of applications such as wireless data transfer, radar systems, and high-data-rate communication [9]. Nevertheless, UWB antennas encounter a notable difficulty in the form of potential interference arising from adjacent narrowband devices that operate within distinct frequency bands. In order to effectively mitigate interference and facilitate uninterrupted UWB communication, it is imperative to incorporate notched-band characteristics into the UWB antenna [10, 11].

A reconfigurable antenna refers to an antenna capable of altering its radiation characteristics, including frequency, radiation pattern, polarization, or impedance, in reaction to control inputs or external stimuli. The capacity to alter and change its attributes renders it a versatile and flexible solution for many wireless communication systems and applications. The main driving force behind the development of UWB reconfigurable antennas is to meet the growing need for wireless devices that can operate in several bands or perform multiple functions. Instead of employing distinct antennas for various frequency bands or applications, a UWB reconfigurable antenna possesses the capability to modify its characteristics in order to encompass several frequency bands or accommodate diverse operating situations [12, 13].

A range of approaches, including the utilization of embedded slots, tapering structures, fractal designs, and defective ground structures, can be implemented to optimize the performance of

* Corresponding author: Dinesh Yadav (dinesh.yadav@jaipur.manipal.edu).

the antenna and get a broad bandwidth. The dimensions and configuration of the ground plane are significant factors in affecting both the radiation properties and impedance matching of the antenna. The notched-band ultra-wideband reconfigurable antenna represents a significant advancement within the realm of antenna design and wireless communication technologies. The growing dependence of our contemporary society on wireless connectivity for many applications has led to an unprecedented need for antennas that can effortlessly adjust to a broad spectrum of frequencies and communication protocols. The advanced antenna technology presents a viable option that may effectively address the increasing need by offering flexibility and adjustability in a continuously developing wireless environment [14–16].

The notched-band is a type of frequency filter that is characterized by its distinctive notched Ultra-Wideband (UWB) technology which refers to a wireless communication technique that utilizes reconfigurable antennas having numerous notable benefits. These devices have a broad range of applications, spanning from Internet of Things (IoT) devices and wireless sensor networks to crucial military and aerospace systems. Through the process of fine-tuning the frequency responses, it becomes possible to augment the quality of signals, mitigate interference, and raise the overall efficiency of wireless communication systems. Designing these antennas poses significant challenges, since it requires intricate engineering expertise to carefully evaluate several factors such as materials, components, and electromagnetic principles. The task of attaining reconfigurability while maintaining optimal performance can provide a significant obstacle. In addition, it is crucial to guarantee adherence to regulatory standards and meet specific application needs. The advancement and implementation of notched-band ultra-wideband reconfigurable antennas are anticipated to play a crucial role in the ongoing progression of wireless communication. With the emergence of novel technologies and the evolution of communication standards, it is anticipated that these antennas will assume an even greater level of indispensability. The notched-band ultra-wideband reconfigurable antenna signifies a significant advancement in the field of antenna technology. The promising potential of this solution lies in its adaptability, versatility, and capacity to function well across a wide variety of frequencies. This makes it well suited to address the numerous and constantly expanding requirements of contemporary wireless systems and applications. As society continues to progress in the era of wireless technology, it is anticipated that these antennas will play a pivotal role in driving innovation and facilitating connectivity.

Ultra-wideband (UWB) monopole antennas exhibit significant versatility in comparison to alternative antenna configurations due to their extensive operational bandwidth, spanning from 3.1 GHz to 10.6 GHz [17]. The performance of these antennas in effectively harnessing the complete UWB spectrum is contingent upon the absence of any adjacent narrowband signals causing interference. However, when narrowband systems such as Wi-MAX (3.3 to 3.6 GHz band), WLAN (5.15 to 5.35 GHz and 5.725 to 5.825 GHz bands), and HIPERLAN (5.45 to 5.725 GHz band) are present, they can affect the UWB system's wide frequency range. To effectively mitigate signal interference, it is important to employ a band-notch UWB antenna. The dimensions of the UWB antenna are limited because of specified performance criteria. Consequently, researchers have turned their attention to reconfigurable frequency antennas, which allow the antenna to change its resonance from one band of operation to another without altering the fabricated prototype. This is achieved using diode switches. Numerous single-fed antenna configurations have been reported in the literature, capable of being switched in one or more bands of operation [18–22]. For instance, in [18], a reconfigurable circular unipolar antenna with a U-shaped slot achieves a single band slot at 3.3–4.1 GHz. Moreover, researchers have explored various designs of printed monopole antennas featuring reconfigurable band-notch capabilities to mitigate signal interference arising from narrowband signals within the frequency range of 3.1 to 10.6 GHz [22–25]. A different methodology entails the incorporation of two slots within the radiating patch and the utilization of two p-i-n diodes to attain adjustable single and dual-band notches. The control over these notches can be achieved by manipulating the bias voltage of the p-i-n diodes, as detailed in [22]. Additionally, [23] presented a single-band reconfigurable slot antenna (5.03–5.94 GHz) equipped with a p-i-n diode switch, offering switchable characteristics within the UWB spectrum and notched-band performance. Furthermore, in [25], researchers harnessed RF microelectromechanical system (MEMS) switches to attain reconfigurable band-notch functionality. A frequency reconfigurable monopole antenna, which is capable to switch from the entire UWB to single band-notched UWB to dual-band radiator controlled by p-i-n diode bias voltage, is reported in [26].

Additionally, a tri-notched coplanar waveguide (CPW)-fed monopole antenna for UWB application is reported in [27] with dual notching elements that cover UWB range of 3.1 to 10.6 GHz, and by utilizing the vector diode tenability of antenna is done. Similarly, a CPW characteristics monopole antenna is presented [28] for WLAN (5.2/5.8 GHz) and Wi-MAX (5.5 GHz) reconfigurable notches with resonant frequency band 3.05 to 12.11 GHz and notch band frequency 3.89 to 5.93 GHz. In [29], a fractal UWB antenna is reported for triple reconfigurable notch reject bands, WiMAX, WLAN, and X-band, applications, Through the incorporation of a split ring resonator and a U-shaped slot, these frequency bands are effectively attenuated or rejected. For reconfigure-ability two diodes are used, and the operating frequency range of antenna is 3.1 GHz to 10 GHz. A dual notch band frequency (4.2–5.2 GHz and 6.2–8.1 GHz) reconfigurable antenna with CPW and a defective ground structure is reported with 2.9 to 12 GHz bandwidth in UWB mode, and reconfigurable switching is done by utilizing four PIN diodes [30]. A similar antenna is reported for WiMAX (3.01–3.63 GHz) and WLAN (4.48–5.85 GHz) notched bands in [31]. A fractal reconfigurable antenna is reported for S (2–4 GHz), C (4–8 GHz), and X (8–12 GHz) microwave bands smart wireless communication. The reconfigurable ability of antenna is achieved by utilizing two PIN diodes [32].

In this communication, circular monopole UWB reconfigurable antenna with wide notched band of 1 GHz ranges from 5 to 6 GHz in UWB band. As a result, in all diodes ON and OFF states, design antenna shows switching of its resonance in

whole UWB to wide notched band UWB applications. The antenna under consideration demonstrates remarkable proficiency in switching its resonance from the ultra-wideband to a single band with notched UWB characteristics. This particular band includes three sub-bands: WLAN (5.15–5.35 GHz and 5.725–5.825 GHz) and HIPERLAN (5.45–5.725 GHz). To achieve this functionality, the antenna employs a biasing circuitry comprising three p-i-n diodes, four inductors, and four biasing pads to provide the necessary DC supply to the diodes.

2. ANTENNA DESIGN AND ANALYSIS

2.1. Designing of a Conventional Circular Monopole UWB Antenna

The initial design process of the basic ultra-wideband monopole antenna began by considering a circular patch structure. To achieve a wide impedance bandwidth, the radius of the circular radiator (a) and the ground plane length (L_g) were set to fixed values of 10.2 mm and 8.2 mm, respectively. A 50-Ω transmission line feeds the antenna, measuring 8.85 mm L_t and 3 mm W_f. The complete antenna simulation was carried out using CST-MWS software [33]. Figure 1(a) depicts the planned circular monopole antenna, and its design takes into account the following parameters:

(i) Antenna dimensions ($L \times W$): $30 \times 24\,\text{mm}^2$
(ii) Patch dimension (a): 9.5 mm
(iii) Substrate material: RT/Duroid 5880 ($\varepsilon_r = 2.2$, $\delta = 0.0009$)
(iv) Substrate thickness (h): 0.79 mm
(v) Length of feed line (L_t): 8.85 mm
(vi) Width of feed line (W_f): 3 mm
(vii) Ground plane length (L_g): 8.2 mm
(viii) Patch-ground gap (g): 0.65 mm

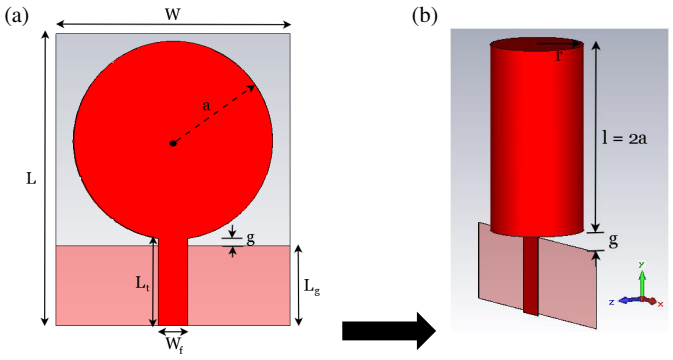

FIGURE 1. (a) The figure illustrates the geometry of a circular patch antenna along with its associated parameters. (b) It depicts a cylindrical monopole antenna with matching height and an equivalent radius, serving as an equivalent to the circular patch antenna.

2.2. Calculation of the Lower Cutoff of the Circular Monopole Antenna

The circular monopole antenna lower cutoff frequency is denoted by 'f_L', which corresponds to a reflection coefficient of less than -10 dB, and its calculation involves setting the area of the circular monopole (πa^2) equal to that of a comparable cylindrical monopole antenna (as illustrated in Figure 1(b)) having the same height and an equivalent radius. The calculation process is described below [34, 35].

$$f_L = \frac{c}{\lambda} = \frac{7.2}{l + r + g}\,\text{GHz} \tag{1}$$

$$2\pi r l = \pi a^2 \tag{2}$$

Here, length (in cm) of the equivalent cylindrical monopole antenna and effective radius (in cm) is denoted by 'l' and 'r', respectively, where $l = 2a$ and $r = a/4$.

$$l = 2a = 2.04\,\text{cm} \tag{3}$$

which gives

$$r = \frac{a}{4} = 0.255\,\text{cm} \tag{4}$$

When evaluating a circular patch that emits radiation, characterized by a radius of $a = 1.02$ cm and a ground patch gap $g = 0.065$ cm, the computed lower cutoff frequency is found to be 3.05 GHz. It verifies that the design parameters are as per the specification of the UWB antenna. Figures 2(a)–(b) show the basic antenna structure without and with stepped feed for the comparison, respectively. The variation of the simulated magnitude of S_{11} with frequency for Ant. 1 is depicted in Figure 3. It is observed that Ant. 1 consists of two operating bands, ranging from 3.4 to 4.8 GHz and 5.4 to 8.2 GHz. Further, to enhance the impedance bandwidth, its feed width is tapered from $W_f = 3$ mm to $W_s = 2$ mm at length $L_f = 2$ mm as displayed in Figure 2(b). The feed line's total length remains constant at $L_t = 8.85$ mm. The intentional adjustment of the feed line's cutting edge serves the dual purposes of expanding the surface current path along the feed line and optimizing the capacitive coupling between the feed line and the ground plane. This strategic modification leads to the attainment of a broader impedance bandwidth. The efficacy of this approach is substantiated by the simulation results depicted in Figure 3 for Antenna 2's S_{11} magnitude plot. The simulated wider impedance bandwidth ranging from 3.2 to 13.5 GHz is achieved. Figures 4(a)–(c) show the simulated E/H-plane radiation pattern of Ant. 2 at 3.8, 6.7, and 10.6 GHz resonant frequencies of the UWB. It is realized that these two-dimensional radiation patterns are nearly omnidirectional in nature and significantly resemble that of a monopole antenna.

The deviation from omnidirectional performance is a crucial specification used to define the pattern characteristics of an omnidirectional antenna. While these antennas are often referred to as omnidirectional, they are actually semi-directional and typically operate over a hemisphere (resembling a conical spiral pattern) or omnidirectional in the azimuth plane. In an ideal scenario, an omnidirectional antenna should receive and transmit equally well over the entire required sector of a sphere. However, achieving this perfect performance is challenging, and some tolerance must be allowed. The deviation from omnidirection refers to the tolerated variation in gain that occurs as a function of azimuth angle, elevation angle, or frequency. Figures 4(d)–(e) display the omni-deviation plots at frequencies of

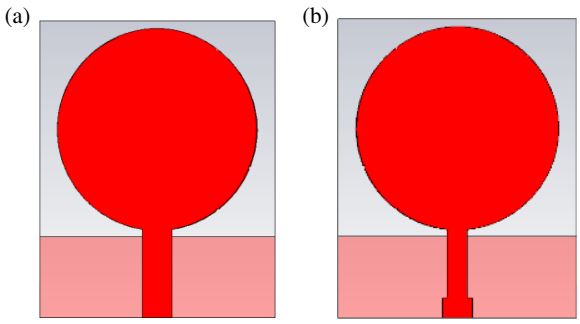

FIGURE 2. (a) Basic circular monopole Ant. 1. (b) Basic circular monopole Ant. 2 with stepped feed.

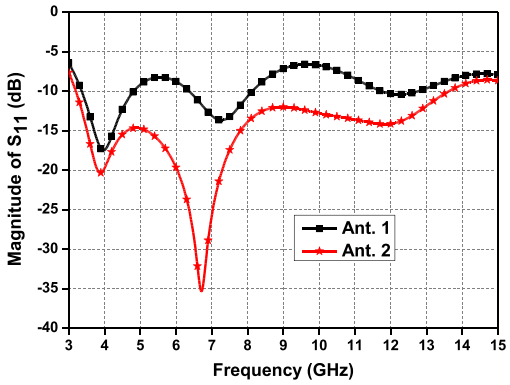

FIGURE 3. The simulated magnitude of S_{11} with frequency for Ant. 1 and Ant. 2.

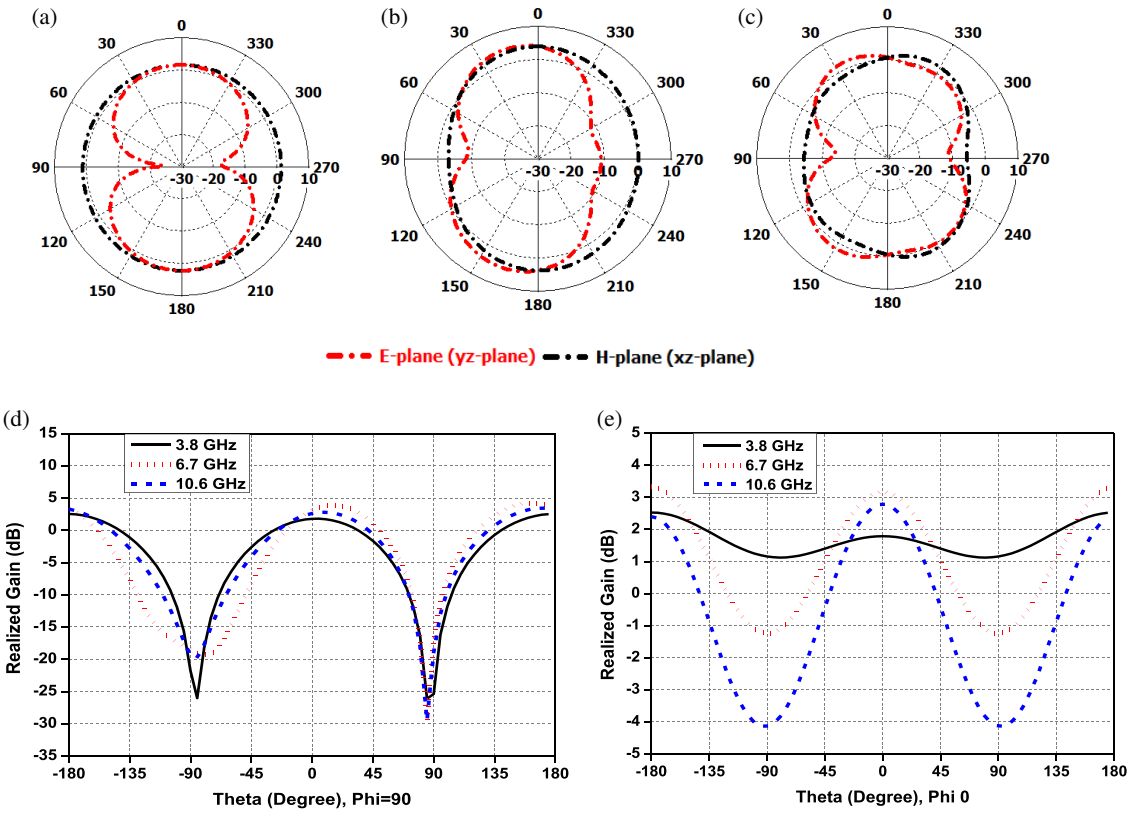

FIGURE 4. The simulated E/H-plane radiation of Ant. 2 at (a) 3.8 GHz, (b) 6.7 GHz, (c) 10.6 GHz and 2D pattern, (d) E-plane, (e) H-plane.

3.8, 6.7, and 10.6 GHz in the E- and H-planes, respectively. It is observed that as the frequency increases, the deviation from the omnidirectional pattern also increases in both the E-plane and H-plane.

2.3. Designing of Reconfigurable Band-Notched UWB Antenna

It is well known for microstrip patch antenna that if the slot is inserted into the main patch to disconnect the section of the patch, the resonant frequency/bandwidth of the antenna will change because the disconnected section behaves like a parasitic element. If we again connect this disconnected parasitic element to the main patch, the antenna will radiate to its original frequency. By applying the same concept to circular monopole antenna, two rectangular vertical slots of the sizes $16.5 \times 0.3\,\text{mm}^2$ and $14.83 \times 0.3\,\text{mm}^2$ are inserted at the positions of 6 mm and 7 mm from the center of the circular patch, respectively, as displayed in Figure 5(a). This leads to decreasing the surface current path of the circular patch. As a result, it is observed that in the same frequency band in UWB spectrum, the magnitude of the S_{11} is less than -10 dB (7.5 to 9 GHz frequency band) in comparison with Ant. 2, which is shown in Figure 6. Further to improve the resonance of the antenna in middle band, a rectangular slot of size $9.2 \times 7.5\,\text{mm}^2$ is inserted at the upper

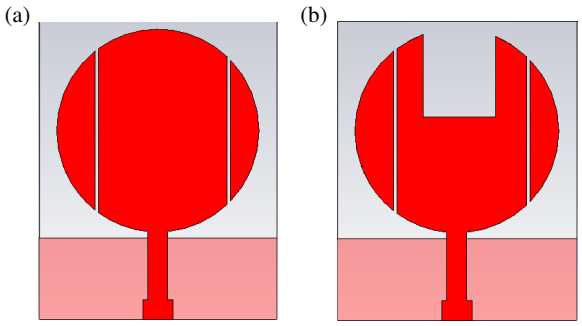

FIGURE 5. (a) Circular monopole Ant. 3 with two vertical slots. (b) Circular monopole Ant. 4 with two vertical slots and rectangular slots.

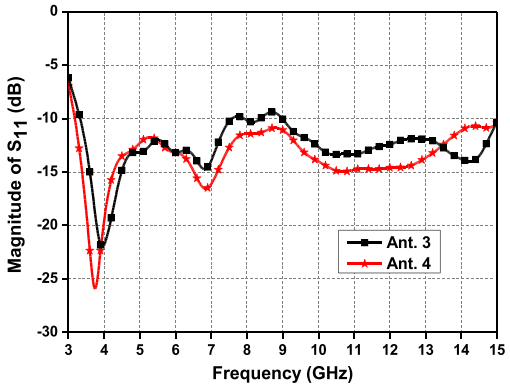

FIGURE 6. Simulated magnitude of the S_{11} plot with frequency for Ant. 3 and Ant. 4.

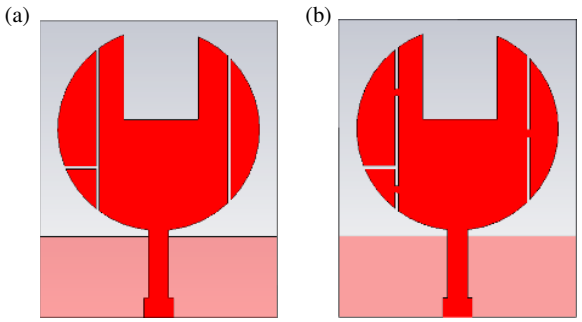

FIGURE 7. The proposed structure of reconfigurable functionality (a) with a horizontal slot, (b) with a horizontal slot and three metallic strips.

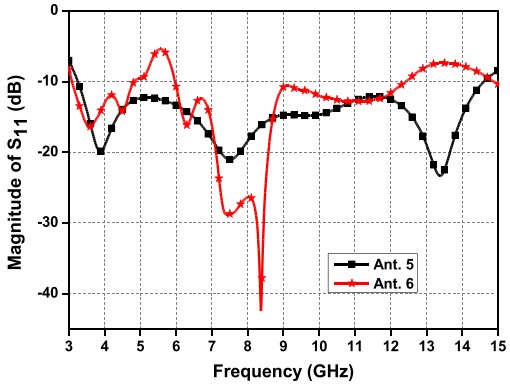

FIGURE 8. The simulated magnitude of the S_{11} plot of the final proposed structures with reconfigurable functionality.

edge of circular patch, which produces asymmetric edges of the slot inside the circular patch of the dimensions $l_4 = 8.58\,\text{mm}$ and $l_5 = 8.38\,\text{mm}$ in length and $W_2 = 7.5\,\text{mm}$ in width, as illustrated in Figure 5(b). The dimensions of the inserted rectangular slot are optimized to achieve an additional resonance from 7.5 to 9 GHz band, as depicted in Figure 6.

Further, to create reconfigurable band-notched characteristics, a horizontal slot of size $0.3 \times 3.2\,\text{mm}^2$ is cut at the position of 4.02 mm above the vertical slot as illustrated in Figure 7(a). These inserted three narrow slots split the circular patch into four sections, which have three parasitic stubs. Additionally, the antenna section which is directly connected to the feed line and remaining three parasitic stubs are utilized to form reconfigurable functionality using diode switches and bias circuitry. The proposed Ant. 5 structure is proficient to radiate from 3.3 to 14.5 GHz including the entire UWB bandwidth, as displayed in Figure 8. Furthermore, three metallic strips of size $0.3 \times 2\,\text{mm}^2$ are inserted in between the vertical slots as shown in Figure 7(b). The position of the strips is carefully adjusted to create a T-shaped slot in the radiating patch, which results in a band-notch at 5.5 GHz. To achieve this, the total length of the inserted T-shaped slot in the radiating patch complies with the $\lambda 5.5\,\text{GHz}/4$ constraint, calculated using Equations (5) and (6). The frequency variation of S_{11} for Ant. 6 is illustrated in Figure 8. The antenna functions within a frequency range spanning from 3.1 to 4.8 GHz and from 6 to 12.5 GHz. Notably, it features a band notch from 4.8 to 6 GHz, which is achieved through the incorporation of a strategically placed T-shaped slot.

$$L_{\text{T-shaped slot at 5.5 GHz}} = \frac{\lambda_g}{4} = \frac{\lambda_0}{4\sqrt{\epsilon_{reff}}} = \frac{c}{4f_{\text{notch}}\sqrt{\epsilon_{reff}}} = W_1 + L_7 = 10.8\,\text{mm} \quad (5)$$

$$\varepsilon_{reff} = \frac{\varepsilon_r + 1}{2} + \frac{\varepsilon_r - 1}{2}\left[1 + 12\frac{h}{w}\right]^{-1/2} \quad (6)$$

Here, free space wavelength ($\lambda_0 = c/f_{\text{notch}}$), speed of light ($c$), notched band center frequency (f'_{notch}), effective permittivity (ε_{reff}), substrate dielectric constant (ε_r), substrate width (w) and substrate hight (h).

The radiation characteristics of Ant. 5 and Ant. 6 are merged in a single antenna by using p-i-n diode switches, which is demonstrated in Figure 9. The proposed antenna structure has three p-i-n diodes (D_1, D_2, and D_3) in place of metallic strips, four inductors (L_1, L_2, L_3, and L_4) of 30 nH each and four biasing pads of size $2 \times 1\,\text{mm}^2$. This design utilizes three p-i-n diodes (MA4SPS402 [36]) to establish and break connections between the isolated stubs and the component of the structure that is directly linked to the feed line. Moreover, inductors are

TABLE 1. Optimized parameters for the proposed reconfigurable antenna.

Parameter	Size (mm)	Parameter	Size (mm)	Parameter	Size (mm)
L	30	L_g	8.2	l_3	14.83
W	24	g	0.65	l_4	8.58
a	10.2	g_1	0.3	l_5	8.38
L_t	8.85	g_2	0.2	l_6	4.7
W_f	3	w_1	2.7	l_7	8.1
L_f	2	w_2	7.5	l_8	2.75
L_s	6.85	l_1	4.02	l_9	7.6
W_s	2	l_2	16.5	l_{10}	7

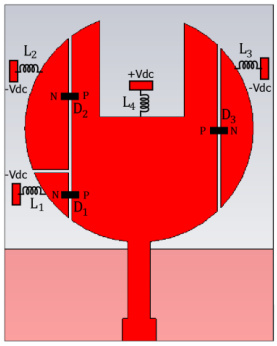

FIGURE 9. Antenna structure with diodes, inductors, and biased circuitry.

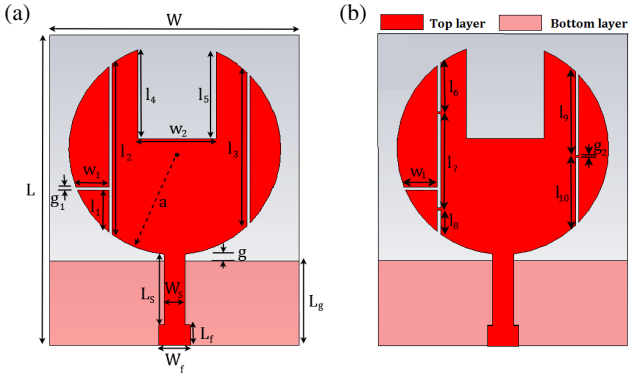

FIGURE 10. Proposed monopole circular UWB antenna structure with parameters (a) OFF-state of all diodes, (b) ON state of all diodes.

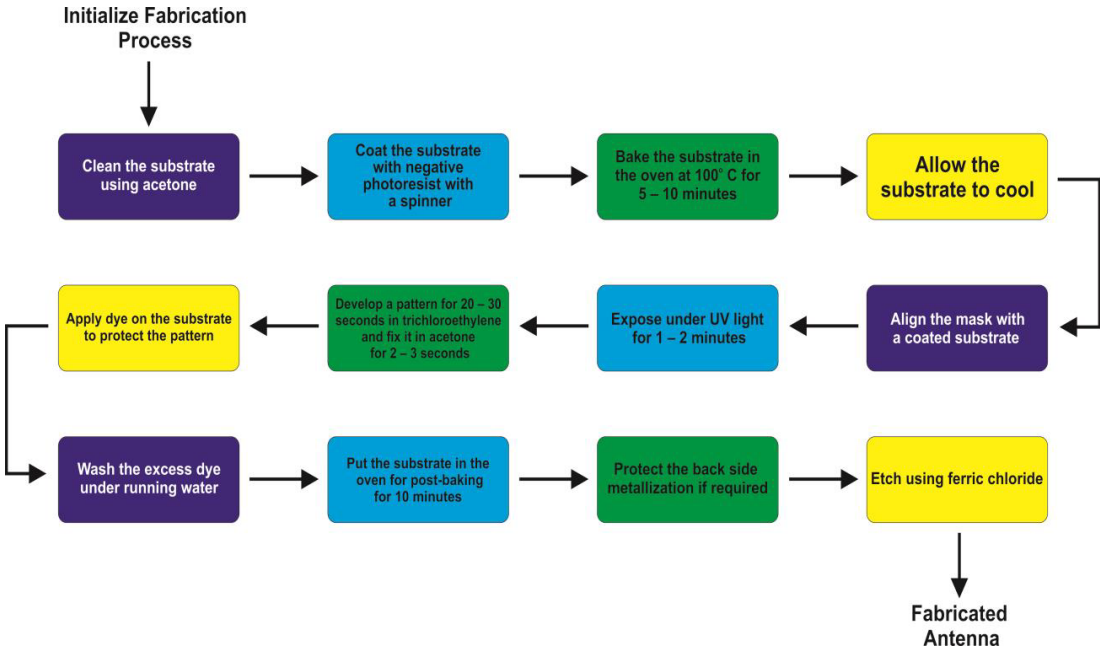

FIGURE 11. Flow chart of the steps to fabricate the antenna.

utilized as radio frequency (RF) chokes within the bias circuit. Figures 10(a)–(b) display the antenna structures with dimensions in diode's ON- and OFF-states, respectively. Table 1 represents the optimized dimensions of the proposed reconfigurable antenna. The flowchart of the steps to fabricate the antenna is shown in the Figure 11. The fabricated proposed reconfigurable antenna with front view consisting of three p-i-n diode switches and four RF-choke inductors is depicted in Fig-

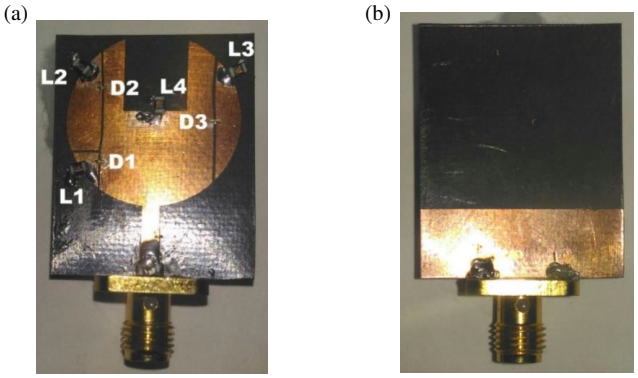

FIGURE 12. Fabricated prototype of the proposed reconfigurable antenna (a) front view with three p-i-n diodes and four inductors, (b) back view.

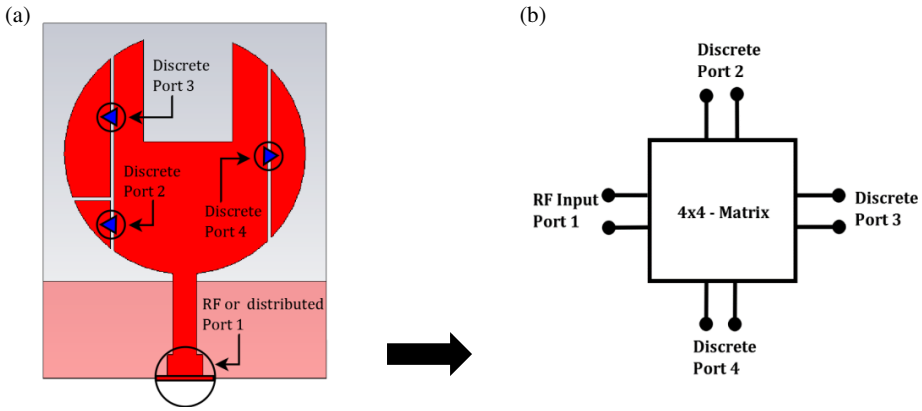

FIGURE 13. Full simulation process of proposed reconfigurable UWB antenna. (a) EM simulation in CST. (b) Circuit simulation in ADS.

ure 12(a), and the back view of proposed antenna is display in Figure 12(b).

2.4. Full Modeling of Reconfigurable UWB Antenna

In this section, the influence of loading diode switches and RF-choke inductors on antenna resonance is analyzed using Advanced Design System (ADS) circuit simulator [37]. In the electromagnetic (EM) simulator (CST), the diode's ON-state is achieved by a connected metallic strip of size $0.3 \times 0.2\,\text{mm}^2$. Moreover, the absence of strips is considered as OFF-state of the diode. This antenna model does not consider the reactive properties of actual diode and inductors. Therefore, the full modeling of a reconfigurable antenna that includes reactive effects of the diode can be accomplished by combining EM simulator and circuit simulator.

Figure 13(a) shows the proposed antenna model consisting of three discrete ports in place of metallic strips and one RF or distributed port. Further, the designed model is simulated by using CST simulator, which provides a 4×4 matrix file of S-parameters. This file is then imported into ADS simulator for full circuit modeling. Figure 13(b) depicts the circuit simulation model in ADS with four ports (three discrete and one distributed), which also comprises the S-parameter file from EM simulator. Figure 14 depicts the equivalent circuit simulation model for the proposed reconfigurable antenna within the ADS simulator.

In circuit model, the input RF-signal is applied to port 1, with 50-Ω matched load. Additionally, each discrete port is connected with a dc power supply, an RF-choke inductor of 30 nH, and a p-i-n diode (model no. MA4SPS402) consisting of actual electrical properties from datasheet [36]. The MA4SPS402 p-i-n diode displays a 0.1 Ω resistance in ON-state, and in OFF-state, it features a parallel combination of a 0.045-pF capacitance and a 20-kΩ resistance. With its lower parasitic inductance at 0.45-nH and impressive 'RC' constant of 0.23-pS, this diode is exceptionally well suited for high-frequency switching applications. Additionally, this diode is compact in size, measuring 1290 µm × 533 µm. The manufacturer suggests employing thermo-compression bonding as the preferred method for attaching it to the printed circuit board (PCB). The ON-state of the p-i-n diode is achieved by applying a DC-bias voltage between 0.7 and 0.9 volts. Alternatively, the OFF-state can be attained with zero bias voltage. Finally, the full modeling solution of the EM simulation and circuit simulation is combined in ADS simulator after postprocessing.

3. RESULTS AND DISCUSSIONS

The return loss measurements are carried out by utilizing the Anritsu MS2028C VNA and radiation parameters like E/H

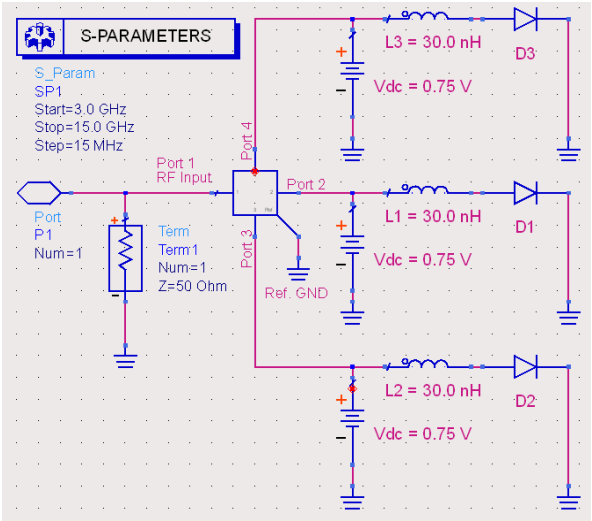

FIGURE 14. Circuit simulation model of the proposed reconfigurable antenna in ADS.

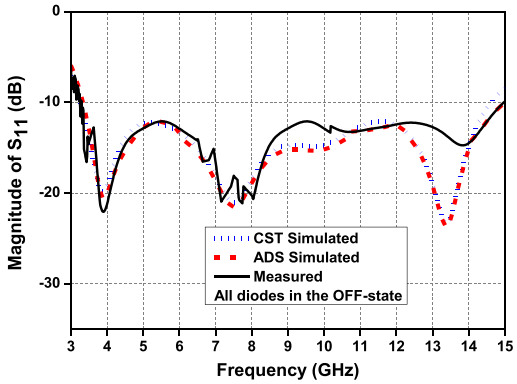

FIGURE 15. The simulated and measured S_{11} plot magnitudes for the proposed antenna with all diodes deactivated (OFF-state).

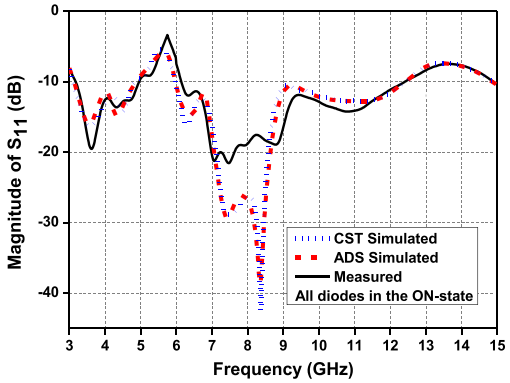

FIGURE 16. The simulated and measured magnitude of the S_{11} plot for the proposed antenna with all diodes activated (ON-state).

field patterns, and gain measurements are done using an anechoic chamber. The comparison of EM simulated (CST), circuit simulated (ADS), and measured magnitudes of S_{11} plots with all the diodes in the OFF-state is shown in Figure 15. The OFF-states of the diodes are achieved in CST by using the disconnected metallic strip, whereas in ADS by applying zero bias voltage to the diodes.

When this diode is in its operational state, it enables a broader impedance bandwidth that encompasses the UWB spectrum, extending from 3.1 to 14.5 GHz. However, with all diodes (D1, D2, and D3) activated in the ON-state, the antenna exhibits a band-notch effect spanning from 5 to 6 GHz, alongside two passbands: one from 3.1 to 5 GHz and the other from 6 to 12.4 GHz, as visually presented in Figure 16. In CST, the ON-state of the diodes could be accomplished by connected metallic strip whereas in ADS it is obtained by applying forward bias voltage 0.75 volts. It is observed that simulation results from both softwares and measured outcomes agree well. The little difference between simulated and measured results may be due to component flaws, fabrication mistakes, and diode biasing feed wires.

Figures 17(a) and 17(b) depict the simulated surface current distribution of the reported antenna operating at a frequency of 5.5 GHz, with all diodes in the OFF-state and ON-state, respectively. It can be seen that in the OFF-state of all diodes, the surface current is almost uniformly distributed along the entire radiating patch, which consists of three slots. When in the ON-state, the predominant concentration of surface current occurs around the T-shaped slots, leading to the emergence of band-notched characteristics centered at a frequency of 5.5 GHz.

Figures 18(a)–(c) compare the proposed antenna's normalized radiation patterns at the operational band's resonant frequencies 3.8 GHz, 6.7 GHz, and 10.6 GHz, respectively. This comparison includes both simulated co-polarized (co-pol) and measured co-polarized (co-pol) and cross-polarized (x-pol) patterns. Interestingly, the state of the diodes (ON/OFF state) does not significantly impact the radiation pattern at these resonant frequencies within the operating band. The radiation patterns in E-plane and H-plane are both almost omnidirectional across the three operating frequencies. The observed maximum levels of cross-polarization (x-pol) in the E-plane and H-plane exhibit values below -30 dB, which signifies excellent perfor-

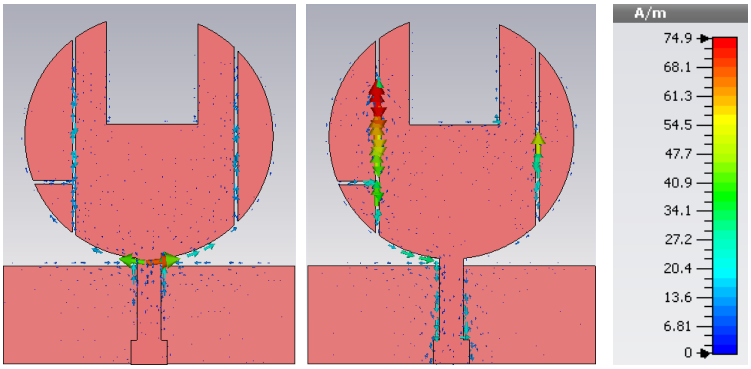

FIGURE 17. Surface current distribution at 5.5 GHz with (a) OFF-state of all diodes, (b) ON-state of all diodes.

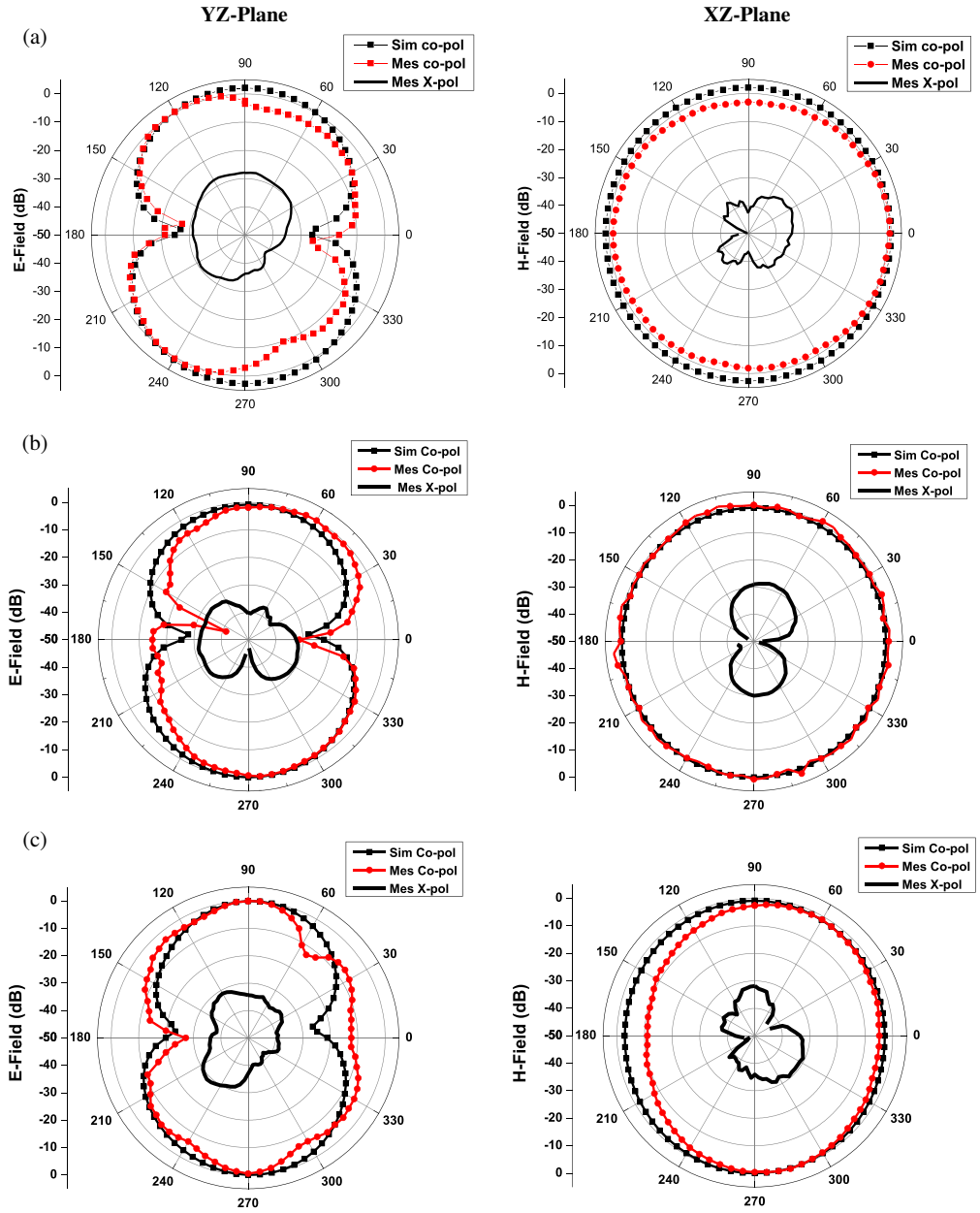

FIGURE 18. The computed radiation patterns of E-plane and H-plane at (a) 3.8 GHz, (b) 6.7 GHz and (c) 10.6 GHz.

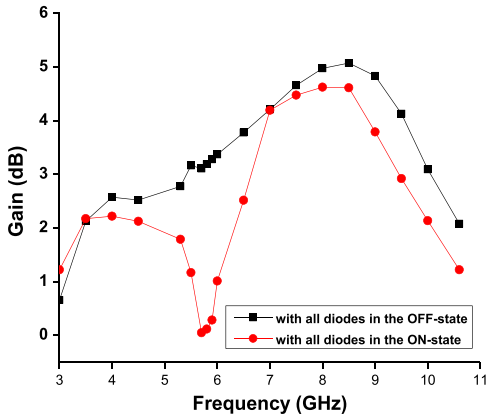

FIGURE 19. Comparison between realized peak gains at different antenna configurations.

TABLE 2. Comparative analysis of present work with previous work.

Ref.	Size (Volume mm^3)	Impedance BW (GHz)	Notch band frequency (GHz)	Notch band Application	Switching capability	Directive Peak Gain (dBi)	Type of Switch
[27], 2018	$36 \times 34 \times 1\,mm^3$	3.1–10.6 GHz	3.97–4.48 GHz, 5.79–6.57 GHz, 7.30–7.60 GHz	narrowband interference, WLAN, X band downlink	Yes	5 dBi	varactor diode
[29], 2019	$21 \times 25 \times 1.6\,mm^3$	3.1–10 GHz	3.3–3.8 GHz, 5.15–5.85 GHz, 8–10 GHz	WiMAX, WLAN and X-band	Yes	—	PIN Diode
[30], 2021	$18 \times 17 \times 1.6\,mm^3$	2.9–12 GHz	4.2–5.2 GHz, 6.2–8.1 GHz	INSAT, 5G and X band	Yes	7.17 dBi	PIN Diode
[31], 2022	$29 \times 35 \times 0.764\,mm^3$	2.6–14.6 GHz	3.01–3.63 GHz, 4.48–5.85 GHz	WiMAX and WLAN	—	3.6 dBi	—
[32], 2022	$32 \times 37 \times 1.6\,mm^3$	2–14 GHz	—	—	yes	—	PIN Diode
[1], 2023	$18.51 \times 22.40 \times 1.6\,mm^3$	7.15–10.925 GHz	—	UWB Application	—	6.99 dBi	—
[7], 2023	$23 \times 38 \times 0.6\,mm^3$	2.4–11.25 GHz	4.4–4.99 GHz, 5.15–5.85 GHz	Mobile Communication and WLAN	—	4.8 dBi	—
This Work	$30 \times 24 \times 0.79\,mm^3$	3–15 GHz	5–6 GHz	WLAN and HIPERLAN	yes	7.64 dBi	PIN Diode

mance. It is noteworthy that the antenna consistently demonstrates omnidirectional pattern across its range of operating frequencies, affirming its practical applicability.

Figure 19 compares the proposed antenna's peak achieved gains with all diodes' OFF and ON states. In the initial configuration, where all diodes are in the OFF-state, the antenna exhibits excellent gain across the entire operational bandwidth, achieving a peak gain of 5.07 dB at 8.5 GHz. However, in the second configuration (with all diodes in the ON-state), a reduction in realized gain is observed within the notched band spanning from 5 to 6 GHz. Across different antenna configurations, the observed realized gains exhibit a constant and uniform pattern at the resonant frequencies within the designated operating band, with the exception of the notched band. It is noteworthy that the inclusion of passive elements, such as diodes and RF-choke inductors, results in a realized gain less than 2 dB at higher frequencies within the ultra-wideband (UWB) spectrum. This observation highlights the influence of these components on the antenna's performance at those frequencies. Comparative analysis of the present work with previously reported work is shown in Table 2.

4. CONCLUSIONS

The study focuses on a circular monopole ultra-wideband (UWB) antenna endowed with reconfigurable band suspension capabilities. It is observed that the antenna efficiently utilizes the entire UWB bandwidth when all diodes are in the OFF-state, and there are no interfering narrowband signals nearby. However, when all diodes are in the ON-state, the antenna achieves a notched band of 1 GHz (5 to 6 GHz) within the UWB. One notable benefit of this design is in its ability to accommodate two distinct working modes through the adjustment of diode bias voltage, without necessitating any modifications to the physical dimensions of the antenna. This reconfigurable functionality makes the antenna highly versatile and suitable for different communication scenarios.

ACKNOWLEDGEMENT

The authors would like to thank the CARE lab, IIT Delhi, India, for their assistance and for providing all the necessary measurement and simulator resources to finish this research.

REFERENCES

[1] Jabeen, S. and G. Hemalatha, "Microstrip fed Pi-slot patch antenna with T-slot DGS for UWB applications," *Progress In Electromagnetics Research C*, Vol. 129, 63–72, 2023.

[2] Maity, B. and S. K. Nayak, "Design of compact CPW-fed symmetrical staircase-shaped UWB antenna using transmission line model," *Progress In Electromagnetics Research C*, Vol. 115, 187–203, 2021.

[3] Bharadwaj, S. S., D. Sipal, D. Yadav, and S. K. Koul, "A compact tri-band frequency reconfigurable antenna for LTE/Wi-Fi/ITS applications," *Progress In Electromagnetics Research M*, Vol. 91, 59–67, 2020.

[4] Srivastava, G., A. Mohan, and A. Chakrabarty, "Compact reconfigurable UWB slot antenna for cognitive radio applications," *IEEE Antennas and Wireless Propagation Letters*, Vol. 16, 1139–1142, 2017.

[5] Yadav, D., M. P. Abegaonkar, S. K. Koul, V. N. Tiwari, and D. Bhatnagar, "A novel frequency reconfigurable monopole antenna with switchable characteristics between band-notched UWB and WLAN applications," *Progress In Electromagnetics Research C*, Vol. 77, 145–153, 2017.

[6] Kumar, A., I. B. Sharma, and M. M. Sharma, "Reconfigurable circular disc monopole UWB antenna with switchable two notched stop bands," in *2016 IEEE Annual India Conference (INDICON)*, 1–4, Bangalore, India, Dec. 2016.

[7] Roy, A., A. K. Biswas, A. Nandi, and B. Basu, "Ultra-wideband flexible wearable antenna with notch characteristics for WLAN applications," *Progress In Electromagnetics Research C*, Vol. 129, 143–155, 2023.

[8] Yadav, D., M. P. Abegaonkar, S. K. Koul, V. Tiwari, and D. Bhatnagar, "A monopole antenna with reconfigurable notched characteristics from WLAN-band notched UWB to ITU-band notched UWB antenna," in *Optical and Wireless Technologies, OWT 2017*, Vol. 472, 647–654, Lecture Notes in Electrical Engineering, Jul. 2018.

[9] Kadam, A. A. and A. A. Deshmukh, "Pentagonal shaped UWB antenna loaded with slot and EBG structure for dual band notched response," *Progress In Electromagnetics Research M*, Vol. 95, 165–176, 2020.

[10] Yadav, D., M. P. Abegaonkar, S. K. Koul, V. Tiwari, and D. Bhatnagar, "A compact dual band-notched UWB circular monopole antenna with parasitic resonators," *AEU-International Journal of Electronics and Communications*, Vol. 84, 313–320, Feb. 2018.

[11] Chen, G., C. Guo, J. Xue, Z. Wang, and M. Pang, "Miniaturized metamaterial ultra-wideband antenna for WLAN and Bluetooth applications," *Progress In Electromagnetics Research C*, Vol. 132, 117–127, 2023.

[12] Sharma, B. L. and D. Mathur, "Ultra-wideband frequency-reconfigurable circular antenna with directional patterns," in *2022 IEEE World Conference on Applied Intelligence and Computing (AIC)*, 497–502, 2022.

[13] Yadav, M. V., S. Baudha, Y. Bansal, and S. K. Verma, "A novel compact rectangular slot antenna with ladder structure for ultra-wideband applications," *Telecommunications and Radio Engineering*, Vol. 81, No. 1, 2022.

[14] Nguyen-Trong, N., A. Piotrowski, and C. Fumeaux, "A frequency-reconfigurable dual-band low-profile monopolar antenna," *IEEE Transactions on Antennas and Propagation*, Vol. 65, No. 7, 3336–3343, Jul. 2017.

[15] Chaouche, Y. B., I. Messaoudene, I. Benmabrouk, M. Nedil, and F. Bouttout, "Compact coplanar waveguide-fed reconfigurable fractal antenna for switchable multiband systems," *IET Microwaves, Antennas & Propagation*, Vol. 13, No. 1, 1–8, Jan. 2019.

[16] Deng, J., S. Hou, L. Zhao, and L. Guo, "A reconfigurable filtering antenna with integrated bandpass filters for UWB/WLAN applications," *IEEE Transactions on Antennas and Propagation*, Vol. 66, No. 1, 401–404, Jan. 2018.

[17] FCC, "First report and order: Revision of Part 15 of the commission's rules regarding ultra-wideband transmission systems," Et Docket 98-153, Washington, DC, Feb. 2002.

[18] Ibrahim, A. A. and R. M. Shubair, "Reconfigurable band-notched UWB antenna for cognitive radio applications," in *2016 16th Mediterranean Microwave Symposium (MMS)*, Abu Dhabi, United Arab Emirates, Nov. 2016.

[19] Tariq, A. and H. Ghafouri-Shiraz, "Frequency-reconfigurable monopole antennas," *IEEE Transactions on Antennas and Propagation*, Vol. 60, No. 1, 44–50, Jan. 2012.

[20] Al-Zayed, A. S., M. A. Kourah, and S. F. Mahmoud, "Frequency-reconfigurable single- and dual-band designs of a multi-mode microstrip antenna," *IET Microwaves, Antennas & Propagation*, Vol. 8, No. 13, 1105–1112, May 2014.

[21] Ojaroudi, N., S. Amiri, and F. Geran, "Reconfigurable monopole antenna with controllable band-notched performance for UWB communications," in *2012 20th Telecommunications Forum (TELFOR)*, 1176–1178, Belgrade, Serbia, Nov. 2012.

[22] Badamchi, B., J. Nourinia, C. Ghobadi, and A. V. Shahmirzadi, "Design of compact reconfigurable ultra-wideband slot antenna with switchable single/dual band notch functions," *IET Microwaves, Antennas & Propagation*, Vol. 8, No. 8, 541–548, Nov. 2013.

[23] Valizade, A., C. Ghobadi, J. Nourinia, and M. Ojaroudi, "A novel design of reconfigurable slot antenna with switchable band notch and multiresonance functions for UWB applications," *IEEE Antennas and Wireless Propagation Letters*, Vol. 11, 1166–1169, Oct. 2012.

[24] Loizeau, S. and A. Sibille, "Reconfigurable ultra-wide band monopole antenna with a continuously tunable band notch," *IET Microwaves, Antennas & Propagation*, Vol. 8, No. 5, 346–350, Oct. 2013.

[25] Nikolaou, S., N. D. Kingsley, G. E. Ponchak, J. Papapolymerou, and M. M. Tentzeris, "UWB elliptical monopoles with a reconfigurable band notch using MEMS switches actuated without bias lines," *IEEE Transactions on Antennas and Propagation*, Vol. 57, No. 8, 2242–2251, Aug. 2009.

[26] Yadav, D., M. P. Abegaonkar, S. K. Koul, V. Tiwari, and D. Bhatnagar, "Frequency reconfigurable monopole antenna with switchable band characteristics from UWB to band-notched UWB to dual-band radiator," in *2016 Asia-Pacific Microwave Conference (APMC 2016)*, New Delhi, India, Dec. 2016.

[27] Rahman, S. U., Q. Cao, Y. Li, I. Gil, and W. Yi, "Design of tri-notched UWB antenna based on elliptical and circular ring resonators," *International Journal of RF and Microwave Computer-aided Engineering*, 1–7, Mar. 2019.

[28] De, A., B. Roy, and A. K. Bhattacharjee, "Design and investigations on a compact, UWB, monopole antenna with reconfigurable band notches for 5.2/5.8 GHz WLAN and 5.5 GHz WiMAX bands," *International Journal of Communication Systems*, Vol. 33, No. 7, May 2020.

[29] Nazeri, A. H., A. Falahati, and R. M. Edwards, "A novel compact fractal UWB antenna with triple reconfigurable notch reject bands applications," *AEU-International Journal of Electronics and Communications*, Vol. 101, 1–8, 2019.

[30] Nan, J.-C., J.-Y. Zhao, and Y. Wang, "A compact dual notch-band frequency reconfigurable UWB monopole antenna," *Progress In Electromagnetics Research M*, Vol. 106, 215–226, 2021.

[31] Venkata, S. G. and S. R. K. Kalva, "UWB monopole antenna with dual notched bands verified by characteristic mode analysis (CMA)," *Progress In Electromagnetics Research C*, Vol. 121, 39–48, 2022.

[32] Masroor, I., J. A. Ansari, A. Pandey, and P. K. Mishra, "Design and analysis of multiband fractal reconfigurable antenna using PIN diodes for smart wireless communications," *Progress In Electromagnetics Research C*, Vol. 120, 209–222, 2022.

[33] CST Studio Suit 2018, Computer Simulation Technology (CST), Darmstadt, Germany.

[34] Gupta, K. C., R. Garg, I. J. Bahl, and P. Bhartia, *Microstrip Lines and Slotlines*, 2nd ed., 10–15, Artech House, 1996.

[35] Kumar, G. and K. P. Ray, *Broadband Microstrip Antennas*, 362–368, Artech House, 2003.

[36] Data sheet at https://cdn.macom.com/datasheets/MA4SPS402.pdf.

[37] https://www.keysight.com/en/pc-1297113/advanced-design-system-ads, 2014.